



A neighborhood evaluated adaptive vector filter for suppression of impulse noise in color images

Zhonghua Ma^{a,*}, Dagan Feng^{a,b}, Hong Ren Wu^c

^aSchool of Information Technologies, University of Sydney, Sydney, NSW 2006, Australia

^bDepartment of Electronic and Information Engineering, Hong Kong Polytechnic University, Hong Kong, Hong Kong

^cSchool of Electrical and Computer Engineering, Royal Melbourne Institute of Technology, VIC 3001, Australia

Available online 29 August 2005

Abstract

A new adaptive vector filter is proposed for impulse noise suppression and its relationship with the recent impulse reduction filters is investigated. The new filter detects outliers presented in the image through a novel neighborhood evaluation process, which significantly improves the accuracy of noise detection and detail preservation. The computational complexity of the new filter is very competitive. Its two parameters can be configured efficiently using online/offline optimization processes. Extensive simulations indicated that the new filter outperforms other prior-art methods in suppressing impulse noise in natural color images.

© 2005 Elsevier Ltd. All rights reserved.

1. Introduction

Color image denosing has attracted increasingly interest during the last decade [1,2]. A major effort has been focused on the vector processing of color data, which takes into account the color inter-channel dependence and thus effectively avoid unpleasant drawbacks (e.g., chromatic shifting) in component-wise filtering techniques [1,3]. Based on the multivariate order statistics (OS) theory [2,4–6], a number of classic vector filters have been advanced, which include the vector median filters (VMF) [7], the vector directional filter (VDF) [8], the directional-distance filter (DDF) [9], and the hybrid directional filter (HDF) [10]. These classic filters are efficient in removing outliers but blur image details due to their pure order statistics approaches. Weighted vector filtering techniques [11–16] have been used to achieve a better detail preservation by utilizing the local spatial relationship of the samples inside the supporting window. Adaptive vector filters [17–22] and fuzzy-based techniques [23–28] were also formulated to cope with the diversities of noise and

image characteristics. For a comprehensive review in this area, refer to [1,2].

In the area of impulse noise suppression, it was found that a key factor to improve the performance of vector filters is to carry out the noise detection in the filtering process. This has been examined in [29–32], where multiple thresholds and corruption detectors are used to locate impulse noise and preserve clean pixels. Recent studies [33,34] also confirmed the superiority of such a multiple threshold-based framework on impulse noise detection and structure preservation. Nevertheless, multiple reference filtering and complex parameter training process highly limited the usage of these filters in real-time application, where the processing time and resource are becoming critical.

Recently, two adaptive vector filters have attracted special research attention due to their excellent performance and low computation complexity. The self-adaptive algorithm (SAA) [35] and the fast adaptive similarity filter (FAS) [36] do not involve any usage of computation-cost reference filter series and multiple thresholds. Instead, they utilize an unique local similarity maximization process to locate the noise and replace the corruption. A high noise detection accuracy is achieved by these filters through adapting its parameter

*Corresponding author. Tel.: +61 2 93513702; fax: +61 2 93513838.
E-mail address: frankma@it.usyd.edu.au (Z. Ma).

online in a very efficient way. However, as the whole noise detection depends on a single adjustable parameter, the filters were found to miss out small impulses and misclassify the detail pixel as noise corruption in many cases.

A new adaptive vector filter is proposed in this paper. The new filter uses a novel two-step impulse detection process to overcome the shortcomings of the FAS/SAA filters. A similarity analysis based on local statistics is first applied to evaluate the noise corruption of each local pixel. Then the information from the neighbors is collected to contribute a final noise decision for each pixel. The miss of small impulses is overcome by the first step, while the chance of misclassifying detail pixels as noise is reduced by the second step. The new filter involves only two parameters, whose optimizing process can be implemented with a high computation efficiency. Noticeable gains have been achieved by the new filter over other prior-art methods in terms of noise detection accuracy, objective measures, and perceptual visual quality.

The paper is organized as follows: Section 2 studies the structure of the FAS/SAA filter. Section 3 presents the formulation of the new filter. Section 4 addresses the parameter optimization method and computation cost of the new filter. Experimental results are presented in Section 5 and conclusions are drawn in Section 6.

2. Review of the FAS/SAA filter

Before the discussion of the SAA filter [35] and the FAS filter [36], some terminologies need to be defined first. Let $\mathbf{x}(\mathbf{c}) = [x^R(\mathbf{c}), x^G(\mathbf{c}), x^B(\mathbf{c})]^T$ denotes a RGB pixel located at coordinate \mathbf{c} , where $\mathbf{c} = \{(c_1, c_2) \mid 1 \leq c_1 \leq H, 1 \leq c_2 \leq W\}$, and H and W are the height and the width of a given RGB image, respectively. Let $\mathbf{W}(\mathbf{c}) = \{\mathbf{x}_0(\mathbf{c}), \mathbf{x}_1(\mathbf{c}), \dots, \mathbf{x}_N(\mathbf{c})\}$ represents a square filter window centered at \mathbf{c} , where $\mathbf{x}_0(\mathbf{c}) \leftrightarrow \mathbf{x}(\mathbf{c})$ is the central pixel (CP) of the window, and $\{\mathbf{x}_i(\mathbf{c}), i = 1, 2, \dots, N\}$ represent other pixels of the window. Fig. 1 illustrates the pixel indices within a 3×3 window where $N = 8$.

$x_1(\mathbf{c})$	$x_2(\mathbf{c})$	$x_3(\mathbf{c})$
$x_8(\mathbf{c})$	$x_0(\mathbf{c})$	$x_4(\mathbf{c})$
$x_7(\mathbf{c})$	$x_6(\mathbf{c})$	$x_5(\mathbf{c})$

Fig. 1. Illustration of pixel indices in a 3×3 -pixel window centered at coordinate \mathbf{c} .

The SAA and the FAS filter adopt a unique noise detecting and filtering approach, which is distinct from the classic multivariate order statistics given by Hardie and Arce [4], Pitas and Tsakalides [5] and Tang [6]. A group of cumulated function, $\{M_k(\mathbf{c}), k = 0, 1, \dots, N\}$, is used by the filters to evaluate the local similarity between a given pixel and other pixels of the window $\mathbf{W}(\mathbf{c})$, which is given by

$$\begin{aligned} M_0(\mathbf{c}) &= \sum_{j=1}^{j=N} \mu[\|\mathbf{x}_0(\mathbf{c}) - \mathbf{x}_j(\mathbf{c})\|], \\ M_k(\mathbf{c}) &= \sum_{j=1, j \neq k}^{j=N} \mu[\|\mathbf{x}_k(\mathbf{c}) - \mathbf{x}_j(\mathbf{c})\|], \end{aligned} \quad (1)$$

where $\|\cdot\|$ denotes a specific vector norm (e.g. L_2 norm), and $\mu(\cdot)$ is a non-ascending similarity function convex on $[0; +\infty)$ and satisfying $\mu(0) = 1$, $\mu(+\infty) = 0$. The filters consider the CP of the window, $\mathbf{x}(\mathbf{c})$, as noise free if and only if $M_0(\mathbf{c}) > M_k(\mathbf{c}), \forall k : 1 \leq k \leq N$. The noisy CP is replaced by a local pixel $\mathbf{x}_m(\mathbf{c})$ which maximizes the value of the cumulated similarity function given by (1), that is,

$$\mathbf{y}(\mathbf{c}) = \mathbf{x}_m(\mathbf{c}) \mid m = \arg \max_i \{M_i(\mathbf{c})\}, \quad (2)$$

while the noise-free CP is left intact to preserve image details.

The difference between the FAS filter and the SAA filter mainly lies in their formulation of the similarity function. Given d as a vector distance and h as an adjustable threshold, the similarity function of the FAS filter is defined as $\mu(d) = 1 - d/h$ for $d \leq h$, and $\mu(d) = 0$, otherwise; while the similarity function of the SAA filter is given as $\mu(d) = \exp\{-\beta d\}$ with β an adjustable shape parameter. Bisection method is used by the two filters to adapt the h or β online to image and noise characteristics [35,36].

A close study of these two filters reveals that the noise detection of the SAA/FAS filter is similar to a threshold process based on a modified multivariate order scheme. Take the FAS filter for example, replacing the $\mu(\cdot)$ of (1) by its similarity function results in the following expressions:

$$\begin{aligned} M_0(\mathbf{c}) &= N - \frac{1}{h} \sum_{j=1}^{j=N} \|\mathbf{x}_0(\mathbf{c}) - \mathbf{x}_j(\mathbf{c})\|, \\ M_k(\mathbf{c}) &= N - 1 - \frac{1}{h} \sum_{j=1}^{j=N} \|\mathbf{x}_k(\mathbf{c}) - \mathbf{x}_j(\mathbf{c})\|. \end{aligned} \quad (3)$$

As such, the condition for a clean CP can be rewritten as $\forall k, 1 \leq k \leq N$

$$\sum_{j=1}^{j=N} [\|\mathbf{x}_0(\mathbf{c}) - \mathbf{x}_j(\mathbf{c})\| - \|\mathbf{x}_k(\mathbf{c}) - \mathbf{x}_j(\mathbf{c})\|] < h. \quad (4)$$

Now, if we define a modified aggregated vector distance (AVD) function as

$$R_k(\mathbf{c}) = \sum_{j=1}^{j=N} \|\mathbf{x}_k(\mathbf{c}) - \mathbf{x}_j(\mathbf{c})\|, \quad 0 \leq k \leq N, \quad (5)$$

then the pixels in the window $\mathbf{W}(\mathbf{c})$ can be ordered as $\mathbf{x}_{(0)}(\mathbf{c}) \leq \mathbf{x}_{(1)}(\mathbf{c}) \leq \dots \leq \mathbf{x}_{(N)}(\mathbf{c})$ if and only if $R_{(0)}(\mathbf{c}) \leq R_{(1)}(\mathbf{c}) \leq \dots \leq R_{(N)}(\mathbf{c})$. In this way, the Eq. (4) above be transformed to a threshold expression of the ordered AVD functions, that is, the CP of the window, $\mathbf{x}(\mathbf{c})$, is noise free if and only if

$$R_{(l)}(\mathbf{c}) - R_{(0)}(\mathbf{c}) < h, \quad (6)$$

where $R_{(l)}(\mathbf{c})$ denotes the ordered AVD function of the CP, i.e., $R_{(l)}(\mathbf{c}) \leftrightarrow R_0(\mathbf{c})$ and $\mathbf{x}_{(l)}(\mathbf{c}) \leftrightarrow \mathbf{x}_0(\mathbf{c})$.

The study above suggests that the aforementioned modified multivariate ordering scheme and the AVD-based threshold operation in (6) constitute the primary factors which contribute to the superior performance of the FAS filter. Since the aggregated distance function $\{R_k(\mathbf{c}), k = 1, 2, \dots, N\}$ is formulated between a local pixel and the neighbors of the local CP, the incorrect multivariate order due to a corrupted CP is avoided [37]. Moreover, as the AVD difference contains more image and noise information than any individual pixel-to-pixel distance, the threshold decision given by (6) may achieve a higher detection accuracy than any impulse detection methods worked on an specific CP-neighbor distance [38].

Other studies have also revealed that many AVD function are highly correlated with the local image structure and noise distribution [6,29,39]. The modified AVD function given by (5) also belongs to this category. So it is very difficult for the FAS/SAA filter to cope with the extensive diversities of the image structure and the noise corruption by adjusting the value of its sole parameter. As a result, two misclassification cases often occurred in the detection process of the FAS/SAA filter, which include: (1) detecting impulses as clean pixels, and (2) detecting image details as impulses. The first error occurs when the CP is located at the center of a smooth image area and corrupted by an impulse noise slightly different from its neighbors. This leads to an increase of the $R_{(l)}(\mathbf{c})$ (the AVD function of the local CP). But the increase is too small to trigger the threshold-based detection (6). The second error often occurs in image areas with sharp edges. As the diversity of the image pixels renders the distribution of the $R_i(\mathbf{c})$ s into a very wide range, the threshold condition of (6) will be met even without any impulse corruption.

3. The proposed filter structure

A new adaptive vector filter structure is proposed in this section to overcome the shortcomings of the FAS/

SAA filter. The filter, named as the *neighborhood evaluated adaptive vector filter* (NEAVF), includes a novel two-step impulse detection module. Local image distribution is included in the local similarity analysis to avoid the error of detecting small impulses as clean pixels, and a neighborhood-based noise evaluation process is introduced to avoid the error of detecting image details as impulses. The proposed filter uses a switched mechanism similar to the FAS/SAA filter. Detected noisy pixels are replaced by one of their neighbors to achieve a maximum local similarity, while noise-free pixels are kept unchanged to preserve the image structures.

3.1. Distribution adapted local similarity analysis

In order to improve the detection accuracy of small impulses, it is desirable to adapt the similarity function to the local image structure distribution. Robust estimation technique has been used to control the structure smoothing effect of the image filtering process [22]. However, the technique only provides an overall estimate for the entire image distribution. Thus, it is not applicable when the image distribution of each local window has to be estimated independently or the computation/memory resource is critical.

In this paper, an alternative method is formulated to estimate local image distributions with a high computation efficiency. The method utilizes the strong correlation between the statistic AVD functions and the local image distribution [29]. Given a local window $\mathbf{W}(\mathbf{c})$ and ordering its modified AVD functions as $\{R_{(k)}(\mathbf{c}), k = 0, 1, \dots, N\}$, the local distribution estimator is given by

$$E(\mathbf{c}) = [R_{(N/2)}(\mathbf{c}) - R_{(0)}(\mathbf{c})], \quad (7)$$

The estimator actually applies the median absolute deviation (MAD) estimate [40] on the ordered modified AVD functions. As any corrupted pixel will render its AVD function to an high ranking order, such a MAD estimate will reject majority of impulse corruptions and reveal image distribution underlaid in the ordered AVD function. Fig. 2 demonstrates the performance of the estimator on the 256×256 -pixel size color image *Lena* corrupted by 10% impulse noise, where the noise corruption was simulated according to the method given in Section 5. Extensive tests have confirmed that the proposed estimator is able to efficiently estimate local image distributions from most impulse noise corruptions with a high accuracy.

In this paper, a nonlinear *distribution adapted local similarity* (DALS) function is formulated to evaluate the similarity of the local CP to its neighbors by utilizing the AVD difference evaluation (6) and image distribution estimator (7). Given a local window $\mathbf{W}(\mathbf{c})$ and ordering its modified AVD functions $\{R_{(k)}(\mathbf{c}), k = 0, 1, \dots, N\}$, the

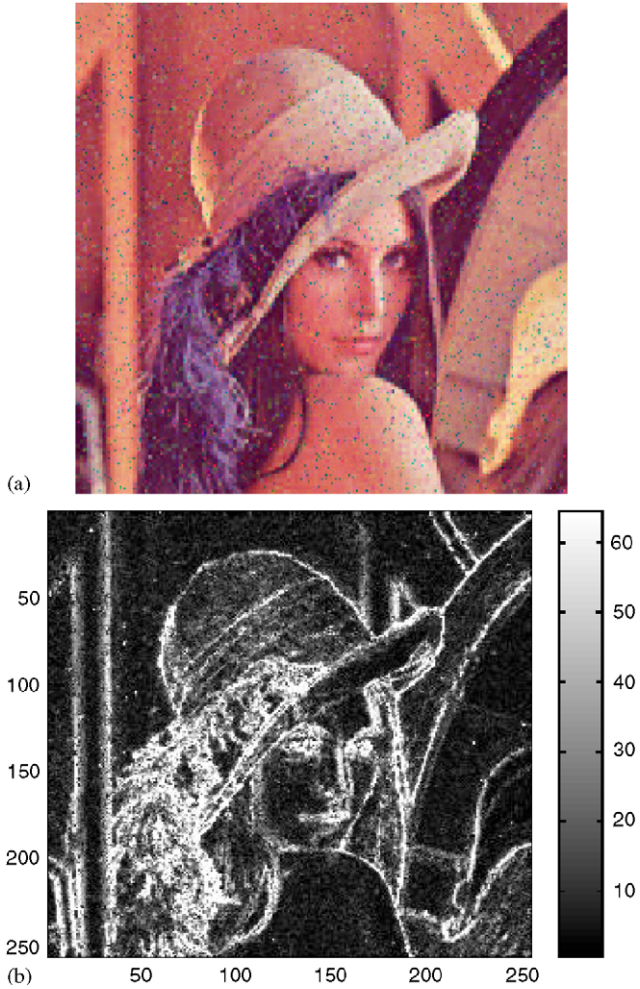


Fig. 2. The performance of the local distribution estimator method on the image *Lena* corrupted by 10% impulse noise. A 3×3 window size is used in the test: (a) corrupted image and (b) estimator output.

proposed DALS function is defined as

$$F_0(\mathbf{c}) = \frac{(2/N)[R_{(N/2)}(\mathbf{c}) - R_{(0)}(\mathbf{c})] + \lambda}{(1/I)[R_{(I)}(\mathbf{c}) - R_{(0)}(\mathbf{c})] + 1.0} \quad (8)$$

if $N/2 \leq I \leq N$, and $F_0(\mathbf{c}) = 1.0$ otherwise, where $R_{(I)}(\mathbf{c}) \equiv R_0(\mathbf{c})$ denotes the ordered AVD function of the local CP, and λ is a parameter adjustable according to the input image and noise characteristics. Please note that the image distribution estimate (7) and the CP-median AVD difference (6) are normalized by their order difference, respectively, in the proposed DALS function. Such a format deliberately utilizes the statistics order information, i.e. the higher the order is, the more likely it resembles an outlier [41]. The denominator is added by 1.0 so that the DALS function does not overflow when $R_{(I)}(\mathbf{c}) = R_{(0)}(\mathbf{c})$.

3.2. Neighborhood evaluated noise detection

The misclassification of pixels as impulse noise often occurs at sharp edge areas. A local window $\mathbf{W}(\mathbf{c})$

placed at a sharp edge usually consists of two distinct pixel groups. The pixel group dominating the local window occupies the local multivariate ranking order from 0 to $N/2$, so $R_{(N/2)}(\mathbf{c}) \approx R_{(0)}(\mathbf{c})$ holds. If the CP belongs to one of the group with less pixels, it usually corresponds to a high ranking order, and results in its AVD function $R_{(I)}(\mathbf{c}) \gg R_{(0)}(\mathbf{c})$. As a result, the DALS function will misinterpret the CP as a strong impulse noise.

An effective technique to cope with such a misclassification is to introduce the *neighborhood evaluation* technique. The technique was first used to design the Kuwahara filter [42] to smooth edge regions damaged by additive noise. In this design, a square symmetric region is divided into four identical sub-windows (or neighborhood windows as named afterward), each containing the CP of the region at one of its corner. The filter replaces the CP by the mean of the most *homogeneous* sub-window. Performance of such a filter was further improved by utilizing more neighborhood window positions and shapes [43], and using a more generalized *confidence value* for the homogeneous evaluation [44]. However, impulse noise is distinct from additive noise in that the noise often disturb local structures and mislead local statistics (e.g., mean or variance). Therefore, the homogeneous of neighborhood windows is very difficult to evaluate for the images corrupted by impulse noise.

An alternative method is developed in this paper to circumvent the difficulty of evaluating the homogeneous window. When we observed a clean pixel using the local statistics in all its neighborhood window, it was found that the pixel always resembles to other clean pixels in several window positions, no matter whether the localized image area is smoothed, or it contains noisy pixels or image details. An example of this case is given in Fig. 3, where the central window (e.g., detection window 1 indicates the CP of the region as an impulse noise. But the evaluations on several other neighborhood windows (e.g., detection window 2 & 3) confirm the CP as a clean pixel.

From the analysis above, an effective impulse neighborhood evaluation is formulated by accumulating all the neighbor local similarity evaluations of the observed pixel to the final noise detection. Let $\mathbf{W}(\mathbf{c})$ denote a window centered at coordinate \mathbf{c} , and $\mathcal{L}(\cdot)$ be a function used to trace the coordinate of the indexed window pixels, i.e., $\mathcal{L}(\mathbf{c}, k) = \mathbf{c}'$ if the pixel coordinate of the indexed window pixel $\mathbf{x}_k(\mathbf{c})$ equals to \mathbf{c}' . The neighborhood impulse evaluation is given by

$$H(\mathbf{c}') = \sum_{\mathcal{L}(\mathbf{c}_k, k) = \mathbf{c}'} [F_k(\mathbf{c}_k)]^\gamma, \quad (9)$$

where $\{\mathbf{c}_k, k = 0, 1, \dots, N\}$ denotes the center coordinate of a neighborhood window which has a window pixel $\mathbf{x}_k(\mathbf{c}_k)$ located on the coordinate \mathbf{c}' ; γ is a parameter used to control the nonlinearity of the neighborhood

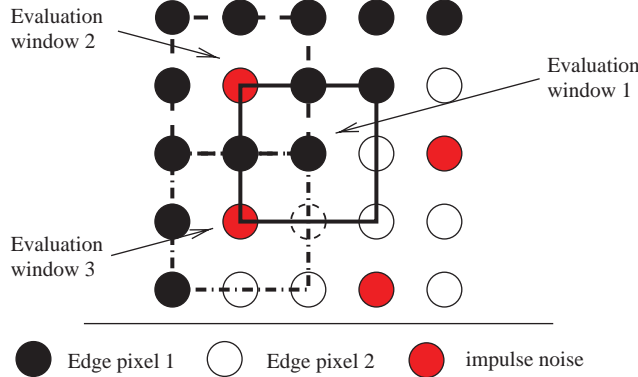


Fig. 3. The neighborhood impulse evaluation on a corrupted sharp edge region. The detection window 1 indicates the CP of the region as an impulse noise. But the detection window 2 & 3 evaluate the CP as a clean pixel.

evaluation. In this paper, $\gamma = 2$ is used throughout the experiments.

The final impulse noise detection is made on the neighborhood evaluation sum $H(\mathbf{c})$ using a binary threshold. The CP, $\mathbf{x}(\mathbf{c})$, is decided to be noise free if and only if $H(\mathbf{c}) \geq \Delta$, where Δ is a *supra-threshold* whose value can be configured efficiently for most natural images and impulse noise ratios.

3.3. The corrupted pixel reconstruction

The noise filtering process uses the switching structure as the FAS/SAA filter. The output is switched between an identity filter and a modified VMF according to the noise decision. Denoting the input pixel value and filtering output at pixel coordinate \mathbf{c} as $\mathbf{x}(\mathbf{c})$ and $\mathbf{y}(\mathbf{c})$, respectively, the proposed switching filtering scheme is defined as follows:

$$\mathbf{y}(\mathbf{c}) = \begin{cases} \mathbf{x}(\mathbf{c}) & \text{if } H(\mathbf{c}) \geq \Delta, \\ \mathbf{x}_{(0)}(\mathbf{c}) & \text{otherwise,} \end{cases} \quad (10)$$

where $H(\mathbf{c})$ and Δ have been defined in Section 3.2, and $\mathbf{x}_{(0)}(\mathbf{c})$ is the vector median obtained by the modified multivariate order statistics in Eq. (5).

4. Parameter optimization and computational analysis

The new filter involves two adjustable parameters, the λ of the DALS function (8) and the Δ used for the neighborhood noise evaluation (10). From a theoretic point of view, these two parameters should be jointly optimized to achieve the best performance. But, such a nonlinear coupled optimization process often incurs a high computational cost, and also easily leads to local minima [45]. In this paper, a decoupled parameter optimization scheme is developed to avoid aforesaid issues. The λ is designed to be updated online using a

cost-efficient bisection method given in Section 4.1, while the supra-threshold Δ is preset during the online updating and adjusted off-line following the method presented in Section 4.2.

4.1. The online optimization of the parameter λ

The parameter λ has a significant impact on the proposed DALS function (8) and the detected noise ratio. When λ is very small, the DALS function reacts sensitively to any local image variations. Therefore, the chance of misclassifying fine pixels as impulse noise is high and the noise ratio is overestimated. On the other hand, when the value of λ is too large, the DALS function often reacts slowly to small impulse noise corruption. As a result, too many impulses are missed and the noise ratio is underestimated.

Our experiment results have revealed that if the new filter is evaluated as a function of λ , the best performance can be well gained when the λ reaches a value which makes the detected noise ratio equal to the actual noise ratio. The results on two 256 × 256-pixel size RGB images *Lena* and *Parrots* are shown in Fig. 4, where 9.51% impulse noise is applied and $\Delta = 4.5$. Such a relationship indicates an effective way to optimize the λ online to achieve the best performance.

The online optimization method of λ is similar to the modified bisection method of the FAS/SAA filter [35,36]. The method is designed to find out the solution of a nonlinear equation given by

$$q(\lambda) - p_v = 0, \quad (11)$$

where $q(\lambda)$ is the percentage of the pixel detected as noise, and p_v is the exact noise ratio which is assumed to be a priori. The optimization method begins with a starting interval $[a, b]$, and terminates when a stop criteria is met. Our tests with a wide range of color images and impulse ratios found that $q(1.0) > 0$ and $q(50.0) < 0$ always hold. Therefore, the searching of the optimal λ value starts within interval of [1.0, 50.0] in this paper.

Fig. 5 illustrates the converge of the optimized method with the *Lena* and the *Parrots* corrupted by 9.51% impulse noise. Given a stop criterion as $\varepsilon = 0.02\%$, the method is able to reach a quite steady solution (e.g., MSE) with less than eight iterations. Tests on other images with different noise corruption also lead to the same conclusion. Thus, in our tests the optimization process is assumed to be finished after eight iterations.

In the applications with the unknown actual noise ratio of the corrupted image, the method formulated by Smolka et al. [35,36] is used to estimate the actual noise ratio from corrupted color images. Tests in [35,36] have confirmed the good performance of estimation method with its two parameters preset as $m = 2$ and $d = 50$.

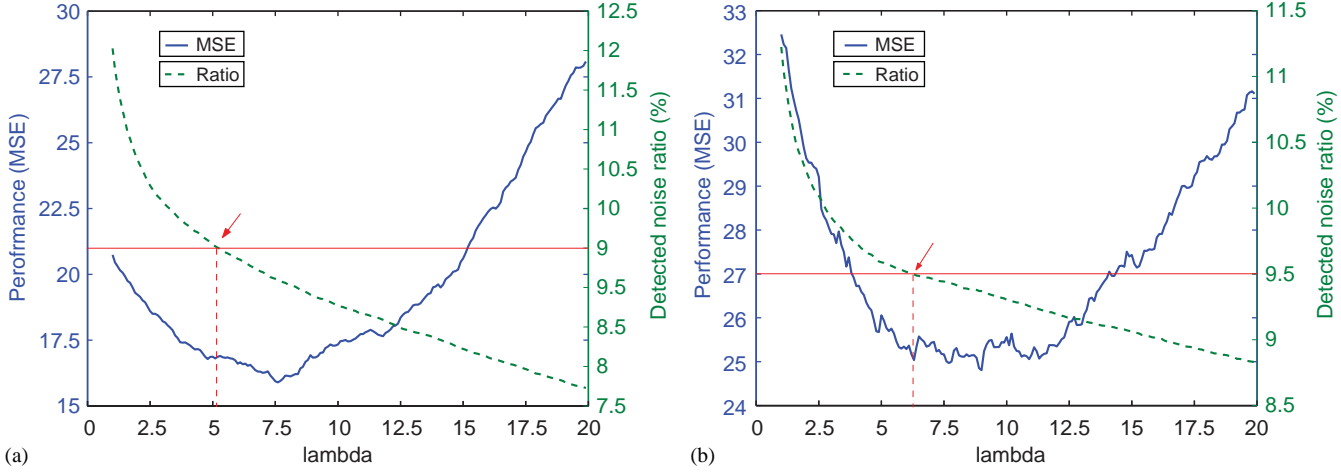


Fig. 4. The correlation between the performance and the detected noise ratio of the new filter, where the image (a) *Lena* and (b) *Parrots* are corrupted by 9.51% impulse noise. The red line indicates the exact noise ratio (e.g., 9.51%). The red arrow highlights the point where the detected noise ratio equals to the exact noise ratio.

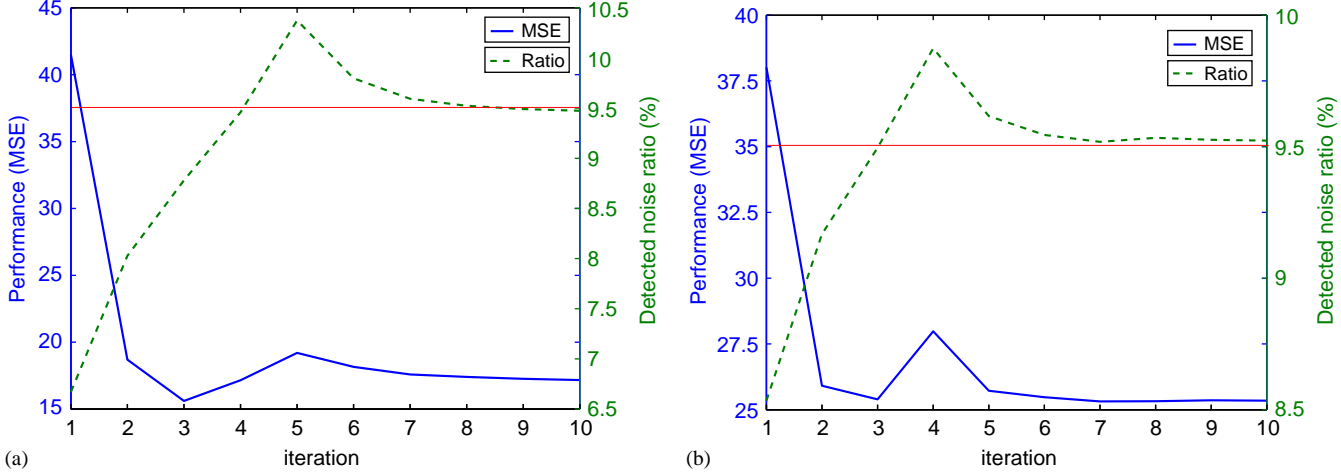


Fig. 5. The correlation between the performance and the detected noise ratio of the new filter, where the image (a) *Lena* and (b) *Parrots* are corrupted by 9.51% impulse noise. The red line indicates the exact noise ratio (e.g., 9.51%).

4.2. The configuration of the parameter Δ

When we address the online optimization of the λ in Section 4.1, the Δ is preset as a fixed value. However, the Δ value affects the performance of the new filter in a noticeable way. Fig. 6 demonstrates the relationship between the parameter Δ and the performance of the filter, where two images, *Lena* and *Parrots*, are corrupted by different degrees of impulse noise and the parameter λ is adapted online using the method afore-addressed. From all the images and noise ratios we examined, the relationship between the parameter Δ and the filter performance depends heavier on the degree of the noise corruption rather than the image characteristics. It is also found that the parameter Δ has less impact on the filter performance when the noise

corruption is low. However, the impact becomes more and more noticeable when the noise corruption increased. Also note that the value of the parameter Δ related to the best filter performance ascends with the increased noise ratio.

The study above results in a noise-dependent scheme for the off-line configuration of the parameter Δ as presented in Table 1. The Δ value is selected according to the input noise ratio. The parameter Δ is preset to a small value when the noise ratio is low. This makes the filtering operation in (10) to prefer the image detail preservation than the noise suppression. The value of the parameter Δ increases with the increased noise ratio, which renders the filtering operation (10) to suppress impulse corruption rather than to preserve image details.

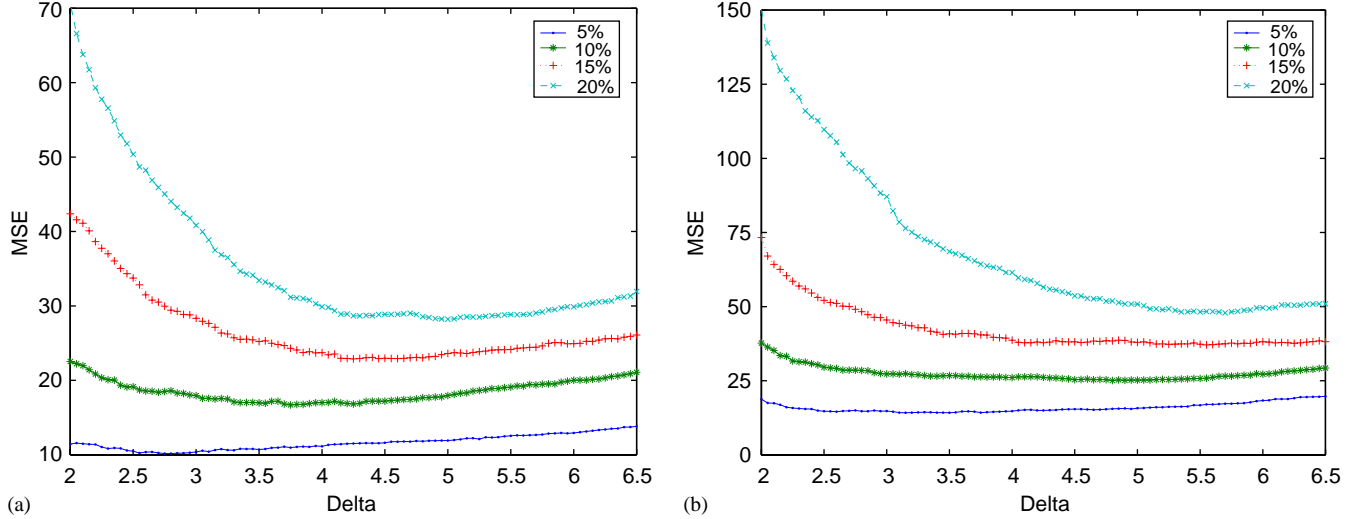


Fig. 6. The relationship between the performance of the new filter and its parameter Δ , where the image (a) Lena and (b) Parrots suffer different percentages of impulse corruption.

Table 1

The recommended Δ value for the NEAVF filter as a function of the input noise ratio

Corruption degree	Low	Moderate	High
Noise ratio (%)	$0 < p_v \leq 5$	$5 < p_v < 15$	$15 \leq p_v$
Recommended Δ	3.0	4.5	5.5

4.3. The computational complexity analysis

A generalized framework has been used to analyze the computational complexity of image filters [13,35,46]. The framework evaluates the computation cost by counting the total elementary operations required in filtering a $n \times n$ -size window containing n^2 vector samples. Elementary operations taken into account consist of additions (*ADDS*), multiplications/divisions (*MULTs*), square roots (*SQRTs*), exponents (*EXPs*), arc cosines (*ARCCOSs*), and comparisons (*COMPs*).

Despite of its two-step impulse noise detection process, the new filter can be implemented in a very cost-efficient way. The entire corrupted image can be processed in a single scan turn, and all the required data can be obtained by calculating the order statistics on each local window once. Details of such an implementation are described as follows:

- The corrupted image is processed by the new filter in a raster scan order, that is, from the left to the right and from the first line to the last line.
- For each local window $W(c)$, the DALS function values of all its window pixels are calculated using Eq. (8) and buffered as $\{F_k(c), k = 0, 1, \dots, N\}$.

(iii) When a pixel coordinate c' has been evaluated in all the possible local windows, its neighborhood evaluation is conducted according to (9) and a noise detection is made accordingly.

(iv) When a noise detection is made for the pixel coordinate c' , its pixel value is reconstructed by the switch-based filtering operation given in (10).

The proposed implementation of the new filter requires the same number of multivariate ranking operations as the FAS filter. The DALS function (8) and the neighborhood noise evaluation (9) of the new filter can be conducted using $O(n^2)$ multiplications, divisions, and additions, respectively. The binary noise detection (10) can be performed with one comparison operation per pixel.

Table 2 presents the cost of the elementary operations for some vector filters, where the Euclidian distance is used by the VMF/SAA/FAS and the NEAVF filter. In our consideration, the parameter estimation of the SAA/FAS/NEAVF filter is bypassed, and the noise ratio is a prior known. It is noted that the new filter maintains the same order of computation complexity as the FAS and the VMF filter. The SAA and the classic basic vector direction filter (BVDF) [8], on the other hand, have to demand additional $O(n^4)$ exponent/arc cosine operations per pixel compared with the VMF/FAS/NEAVF filter.

Real image denoising applications often demand both the noise estimator and the online parameter optimization to be active. In such a case, a fast solution [35,36] has been developed to balance the computation cost and the filter performance. The solution estimates the noise ratio and optimize the parameter online by utilizing only a small part of the corrupted image (i.e., 100×100

pixels for a 512×512 -size image). Tests conducted in [35,36] as well as our own tests have confirmed that such a solution only increases a negligible amount of execution time while the performance of the filter remains almost the same.

5. Simulation and discussion

The impulse noise corruption is applied to test color images according to the model proposed by Lukac et al. [14], Ma et al. [22], and Lukac [31,32]. Denoting the $\mathbf{s}(\mathbf{c})$ and the $\mathbf{x}(\mathbf{c})$, respectively, as the original pixel and the sample pixel at the pixel coordinate \mathbf{c} , and using p_v to determine the noise ratio (the percentage of the corrupted pixels in a given image), the impulse noise corruption is modelled as

$$\mathbf{x}(\mathbf{c}) = \begin{cases} \mathbf{v}(\mathbf{c}) & \text{with probability } p_v, \\ \mathbf{s}(\mathbf{c}) & \text{with probability } 1 - p_v, \end{cases} \quad (12)$$

where $\mathbf{v}(\mathbf{c}) = [v^R(\mathbf{c}), v^G(\mathbf{c}), v^B(\mathbf{c})]^T$ denotes a noise vector suffered from impulse noise corruption on at least one of its components. The impulse corruption is simulated by a two-step method [8,22,23] which takes into account the channel correlation of the impulse corruption. Given a preset noise ratio p_v , the 24-bit RGB image is first corrupted by random impulses from $[0, 255]$ in an component independent manner. Then a factor $\rho = 0.5$ is used for the channel correlation simulation for each

corrupted pixel, that is, if the pixel is corrupted by random impulses on at least one of its components, then its noise-free components have a 50% probability to be corrupted as well.

Several objective criteria are used in our tests to measure the distortion of the vector filters, which include the mean square error (MSE), the mean absolute error (MAE), and the normalized color difference (NCD). The MSE and MAE are defined in the RGB color space and given as follows [31,32]:

$$MSE = \frac{1}{mHW} \sum \|\mathbf{s}(\mathbf{c}) - \mathbf{y}(\mathbf{c})\|_2^2, \quad (13)$$

$$MAE = \frac{1}{mHW} \sum \|\mathbf{s}(\mathbf{c}) - \mathbf{y}(\mathbf{c})\|_1, \quad (14)$$

where $\mathbf{s}(\mathbf{c})$ and $\mathbf{y}(\mathbf{c})$ are, respectively, the original pixel and the restored pixel at pixel coordinate \mathbf{c} ; W and H are the width and the height of the test image, respectively; and m represents the number of color channels. Please note that $\|\cdot\|_2$ denotes the l_2 norm (Euclidean distance) and $\|\cdot\|_1$ denotes the l_1 norm (City-block distance). The NCD measures the color distortion in the perceptual uniform *CIELUV* color space and is defined by [1,32]

$$NCD = \frac{\sum \|\Delta E_{LUV}(\mathbf{c})\|_2}{\sum \|E_{LUV}(\mathbf{c})\|_2}, \quad (15)$$

where for each pixel coordinate \mathbf{c} in the *CIELUV* color space, $E_{LUV}(\mathbf{c})$ and $\Delta E_{LUV}(\mathbf{c})$ represent the magnitude of the original pixel and the difference between the original pixel and its reconstruction, respectively.

Table 2
The computational cost of the NEAVF filter compared with other techniques

Oper.	<i>ADDs</i>	<i>MULTs</i>	<i>SQRTs</i>	<i>COMPs</i>	<i>EXPs</i>	<i>ARCCOSs</i>
VMF	$O(n^4)$	—	$O(n^4)$	$O(n^2)$	—	—
BVDF	$O(n^4)$	$O(n^4)$	$O(n^4)$	$O(n^2)$	—	$O(n^4)$
SAA	$O(n^4)$	$O(n^4)$	$O(n^4)$	$O(n^2)$	$O(n^4)$	—
FAS	$O(n^4)$	$O(n^4)$	$O(n^4)$	$O(n^2)$	—	—
NEAVF	$O(n^4)$	$O(n^4)$	$O(n^4)$	$O(n^2)$	—	—

Table 3
The detection accuracy of different vector filters using the image *Parrots* corrupted by various percentages of impulse noise, where Err-I represents detecting clean pixels as noise, and Err-II represents detecting noise as clean pixels

Filters	0.5%		2%		5%		10%		15%		20%	
	Err-I	Err-II										
AVLUM	281	48	272	42	279	119	289	273	304	509	306	657
AVMF	639	71	621	63	633	161	621	333	587	539	607	617
SCWVDF	63	19	61	32	60	98	65	217	56	407	53	585
FAS	132	89	125	117	194	192	297	297	380	380	432	433
SAA	303	45	299	41	160	156	241	241	302	301	364	358
NEAVF	59	59	58	58	98	98	164	162	240	242	281	279

A 3×3 window size is used by all the filters.

5.1. Results with the test image Parrots

The results on the 256×256 -pixel size color image *Parrots* are highlighted in this section. The specific

spectral (color) characteristics of this test image puts a greater challenge on structure preservation of the vector filters than most other test images. The image has been corrupted by different levels of impulse noise. However,

Table 4

The performance of different vector filters on restoring the image *Parrots* corrupted by various percentages of impulse noise, where a 3×3 window size is used

Filters	0.5%			2%			5%			10%			15%			20%		
	MSE	MAE	NCD	MSE	MAE	NCD	MSE	MAE	NCD	MSE	MAE	NCD	MSE	MAE	NCD	MSE	MAE	NCD
VMF	52.6	2.30	0.014	52.9	2.35	0.014	56.7	2.49	0.015	61.7	2.67	0.016	70.1	2.92	0.018	81.2	3.18	0.020
BVDF	87.5	3.00	0.015	89.4	3.07	0.015	95.2	3.22	0.016	100.0	3.39	0.018	111.7	3.62	0.019	124.2	3.90	0.022
GVDF	67.0	2.92	0.016	66.8	2.98	0.016	69.9	3.14	0.017	74.1	3.42	0.019	80.1	3.76	0.021	93.8	4.19	0.025
DDF	59.2	2.39	0.013	59.0	2.42	0.013	62.8	2.53	0.014	64.4	2.68	0.015	69.6	2.87	0.017	83.1	3.17	0.020
AVLUM	20.2	0.30	0.0012	20.8	0.36	0.0016	25.3	0.50	0.0027	32.2	0.75	0.0047	44.8	1.09	0.0074	57.3	1.38	0.0101
AVMF	32.3	0.56	0.0022	32.5	0.60	0.0025	36.5	0.74	0.0037	42.4	0.98	0.0057	51.6	1.25	0.0080	62.7	1.54	0.0104
ACWVDF	5.3	0.09	0.0004	10.0	0.18	0.0009	19.6	0.39	0.0019	37.4	0.72	0.0037	67.6	1.16	0.0061	97.4	1.59	0.0090
SCWVDF	5.2	0.08	0.0004	9.9	0.18	0.0008	19.6	0.37	0.0018	36.7	0.70	0.0037	68.4	1.15	0.0062	98.6	1.58	0.0093
SAA	8.7	0.15	0.0006	13.3	0.21	0.0010	23.1	0.42	0.0020	32.6	0.69	0.0042	42.6	0.96	0.0058	54.7	1.22	0.0081
FAS	16.4	0.21	0.0011	18.1	0.28	0.0016	26.5	0.48	0.0029	36.8	0.77	0.0057	46.6	1.06	0.0066	61.0	1.36	0.0087
NEAVF	8.6	0.11	0.0005	10.1	0.16	0.0009	15.4	0.32	0.0020	25.3	0.56	0.0037	37.3	0.86	0.0058	48.2	1.10	0.0078

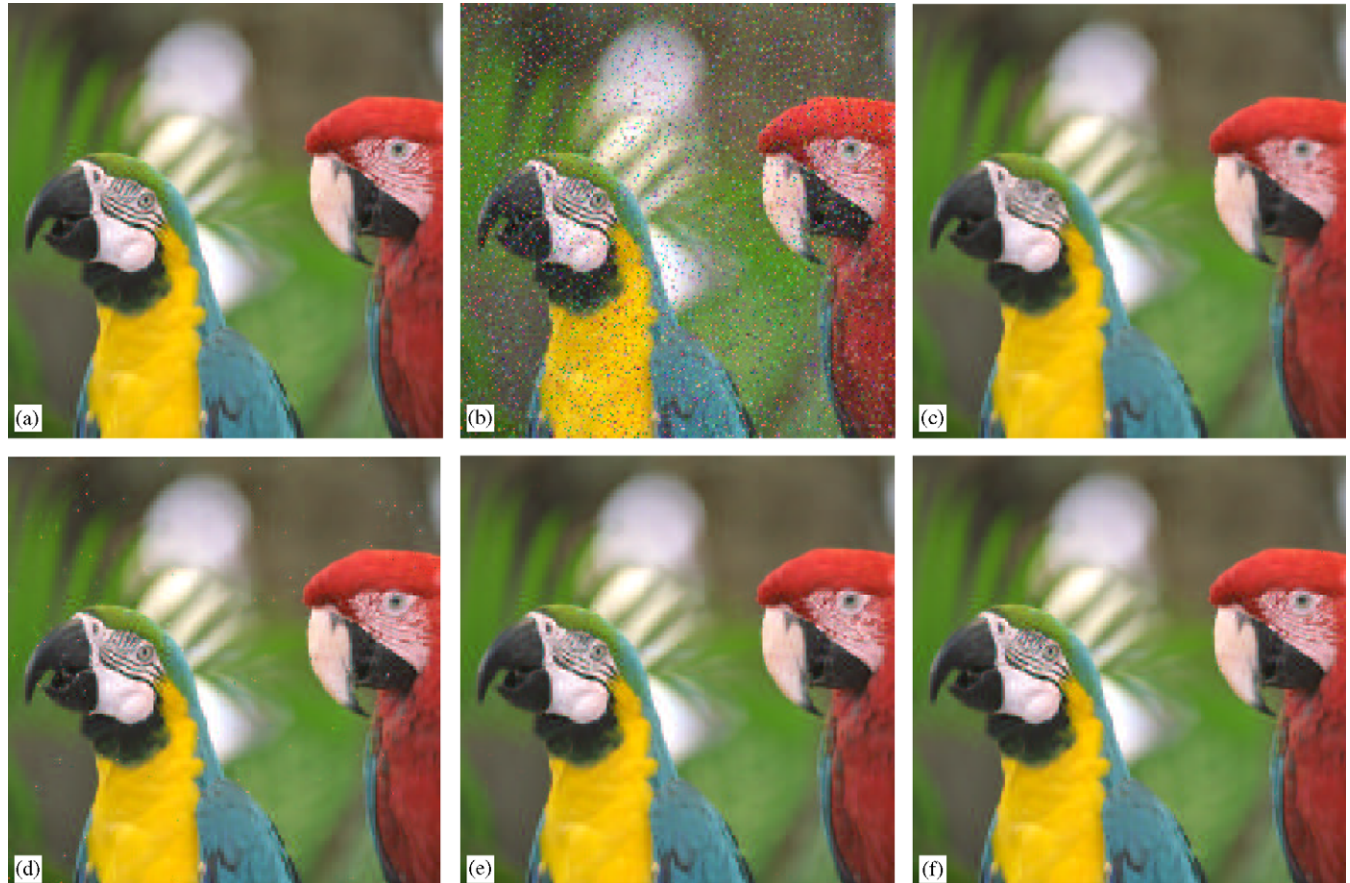


Fig. 7. Reconstructions of the new filter (NEAVF) compared with other techniques, where the image *Parrots* was corrupted by 10% impulse noise and a 3×3 -pixel window is applied: (a) original, (b) corrupted (10% impulses), (c) VMF output, (d) SCWVDF output, (e) SAA output and (f) NEAVF output.

only the results with 0.5%, 2%, 5%, 10%, 15% and 20% noise corruption are demonstrated in this paper due to the page limitation. Several prior-art selective vector filters are used for performance comparisons, which include the adaptive vector LUM smoother (AVLUM) [30], the adaptive vector median filter (AVMF) [31], the selection center-weighted vector directional filter (SCWVDF)/adaptive center-weighted vector directional filter (ACWVDF) [32], the SAA filter [35], and the FAS filter [36]. Parameter settings as proposed in the original works are used by the AVLUM filter, the AVMF filter, and the SCWVDF/ACWVDF filter during the tests. The noise estimator is bypassed in the SAA filter, the FAS filter, and the new NEAVF filter. In these schemes, a priori information about the noise corruption was used.

Table 3 shows the detection accuracy of several vector filters using the image *Parrots* corrupted by different

percentages of impulse noise. Following the evaluation procedures in [32], two specific error measures are used. The *Err-I* recodes the occurrence of detecting clean pixels as impulses, while the *Err-II* recodes the occurrence of detecting impulses as clean pixels. The results reveal that the AVLUM and the AVMF misclassify many clean pixels in low levels of noise corruption, while the SCWVDF tends to miss noise as the corruption level increased. Excellent balance has been achieved by the FAS, the SAA, and the NEAVF filter due to their online parameter optimization technique. As to the NEAVF, its advanced distribution adaption and neighbor evaluation techniques have greatly improve the accuracy of detail preservation and noise detection, resulting in a performance much better than the FAS and the SAA filter in term of the *Err-I* and the *Err-II* measures in all the tested cases.



Fig. 8. The zoomed part of selected reconstructions from Fig. 7: (a) the SCWVDF, (b) the SAA and (c) the NEAVF.

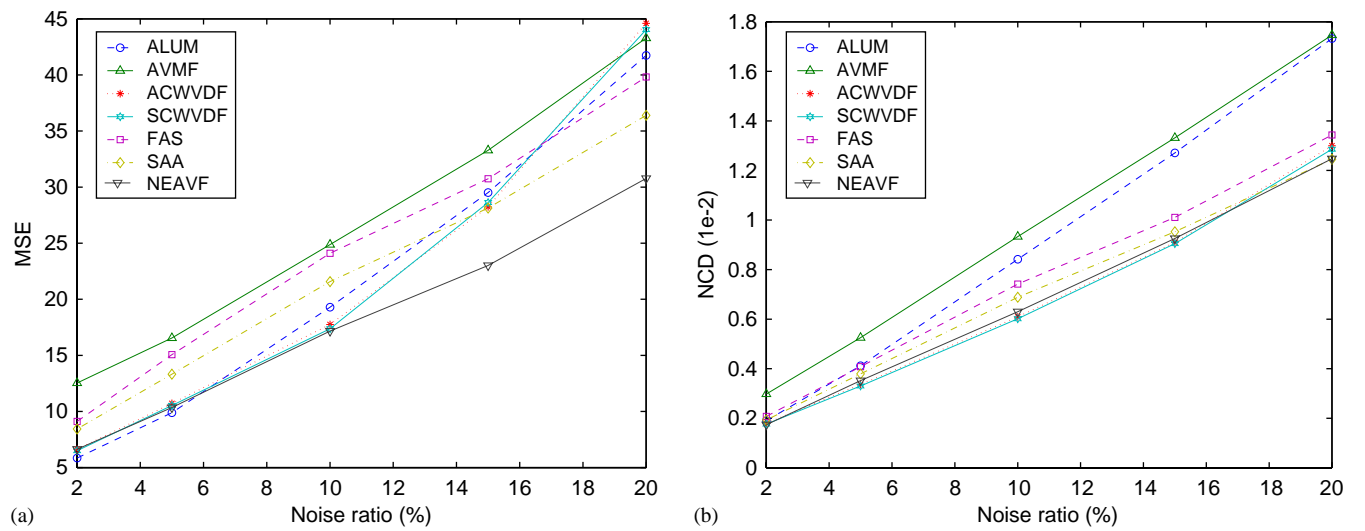


Fig. 9. The distortion measures of different vector filters in terms of (a) the MSE and (b) the NCD, where the image *Lena* suffers different percentages of impulse corruption.

Table 4 presents the performance of the new filter compared with other vector filters on the *Parrots* suffered from different percentages of impulse corruption. All switching vector filters have achieved better

performance than the classic vector filter such as the VMF [7], the BVDF (basic vector direction filter)/GVDF (generalized vector direction filter) [8], and the DDF [9]. The ACWVDF/SCWVDF has demonstrated excellent

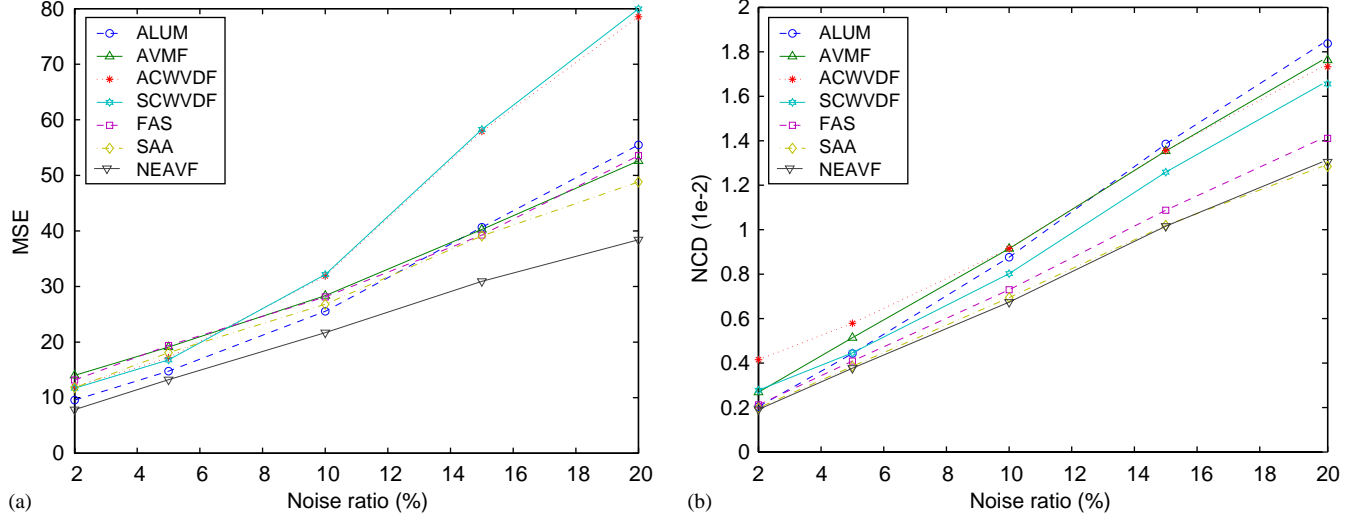


Fig. 10. The performance of the filters in terms of (a) the MSE and (b) the NCD, where the image *Peppers* suffers different percentages of impulse corruption.

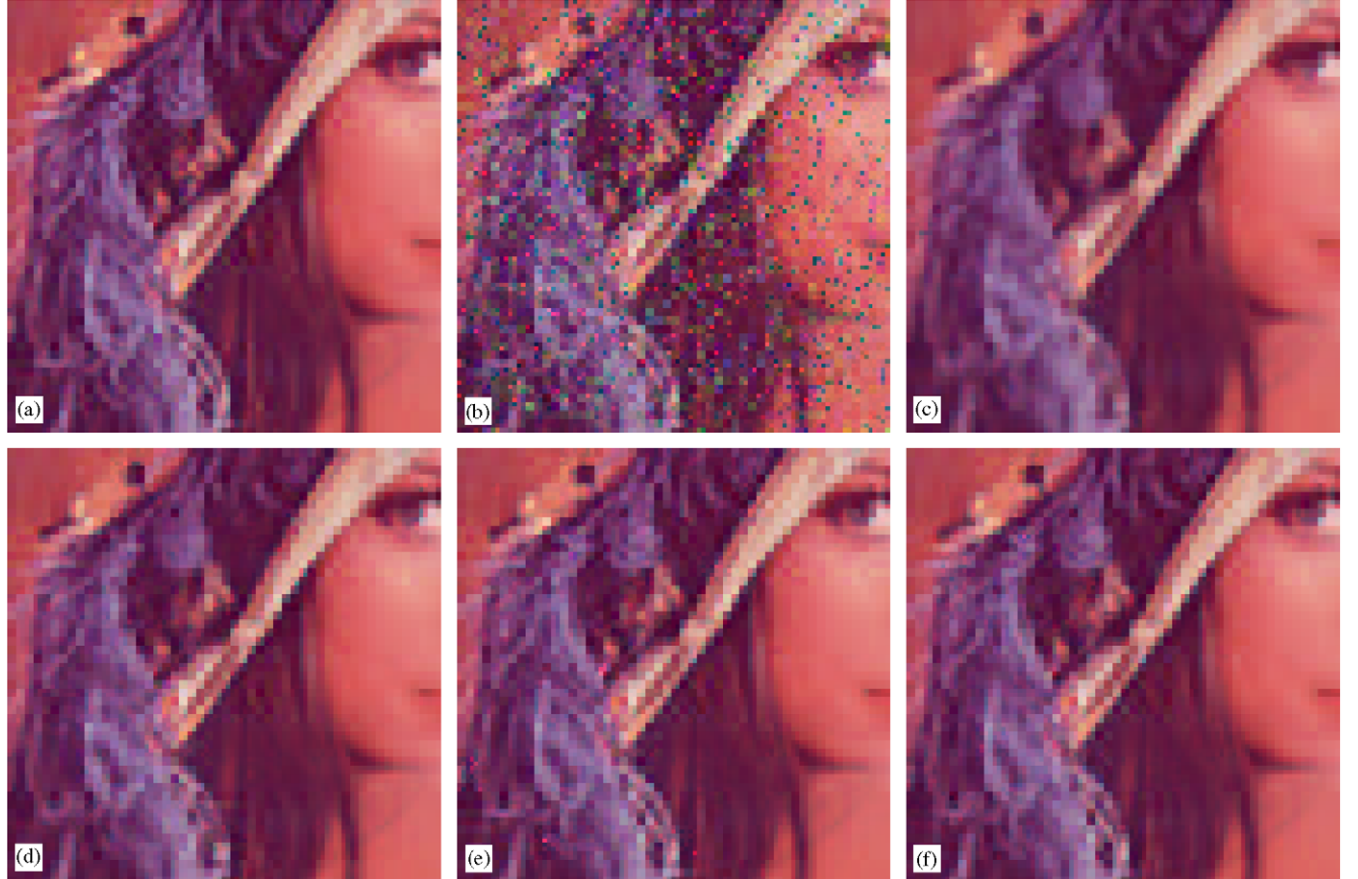


Fig. 11. The zoomed reconstruction of the NEAVF filter compared with other techniques, where the image *Lena* is corrupted by 20% impulse noise: (a) original, (b) corrupted, (c) VMF output, (d) SAA output, (e) SCWVDF output and (f) NEAVF output.

performance in cases of low impulse corruption, while the AVLUM/AVMF/FAS/SAA filter performed quite robust in moderate and high impulse corruptions. It is noted that the proposed filter always achieved the top performance in all concerned noise ratios and that noticeable gains have been observed compared with the SAA/FAS filter on all three objective measures.

Fig. 7 shows the reconstructed image of several vector filters using the image *Parrots* corrupted by 10% impulse noise. The SCWVDF still remains some Salt-like impulses in the background area of its reconstructed image, and the SAA damages sharp image details of the birds. It is obvious that the new filter achieves the best tradeoff between the noise suppression and the detail preservation. The concerned stripe structures and eyes of the birds are preserved as good as those of the SCWVDF, while most of impulses that significantly impact perceptual quality have been removed effectively (please refer to **Fig. 8** for a closer observation).

5.2. Results on other test images

Besides the tests with the image *Parrots*, the new filter was also undertaken comprehensive tests on other color

test images in a wide range of corruption cases. Figs. 9 and 10 present part of the results on two 256-pixel RGB images, *Lena* and *Peppers*, respectively, with 2%, 5%, 10%, 15% and 20% impulse noise corruption. The proposed filter has achieved a better performance than the FAS/SAA filter in term of the MSE/NCD measures in all the test cases. It also exhibited the best robustness among all the test vector filters regarding to different test images and noise ratios. Moreover, **Figs. 11** and **12** highlight some image structures restored by the new filter and its counterparts under variant noise corruption. The proposed NEAVF preserved more image details and structures than the SAA filter, and suppressed more impulses in smooth areas than the SCWVDF. All these contribute to a more pleasant perceptual quality to the reconstructions of the NEAVF than those of its counterparts.

6. Conclusion

A new adaptive vector filter is presented in this paper for color image denosing. The filter utilizes a novel neighborhood impulse evaluation process to improve

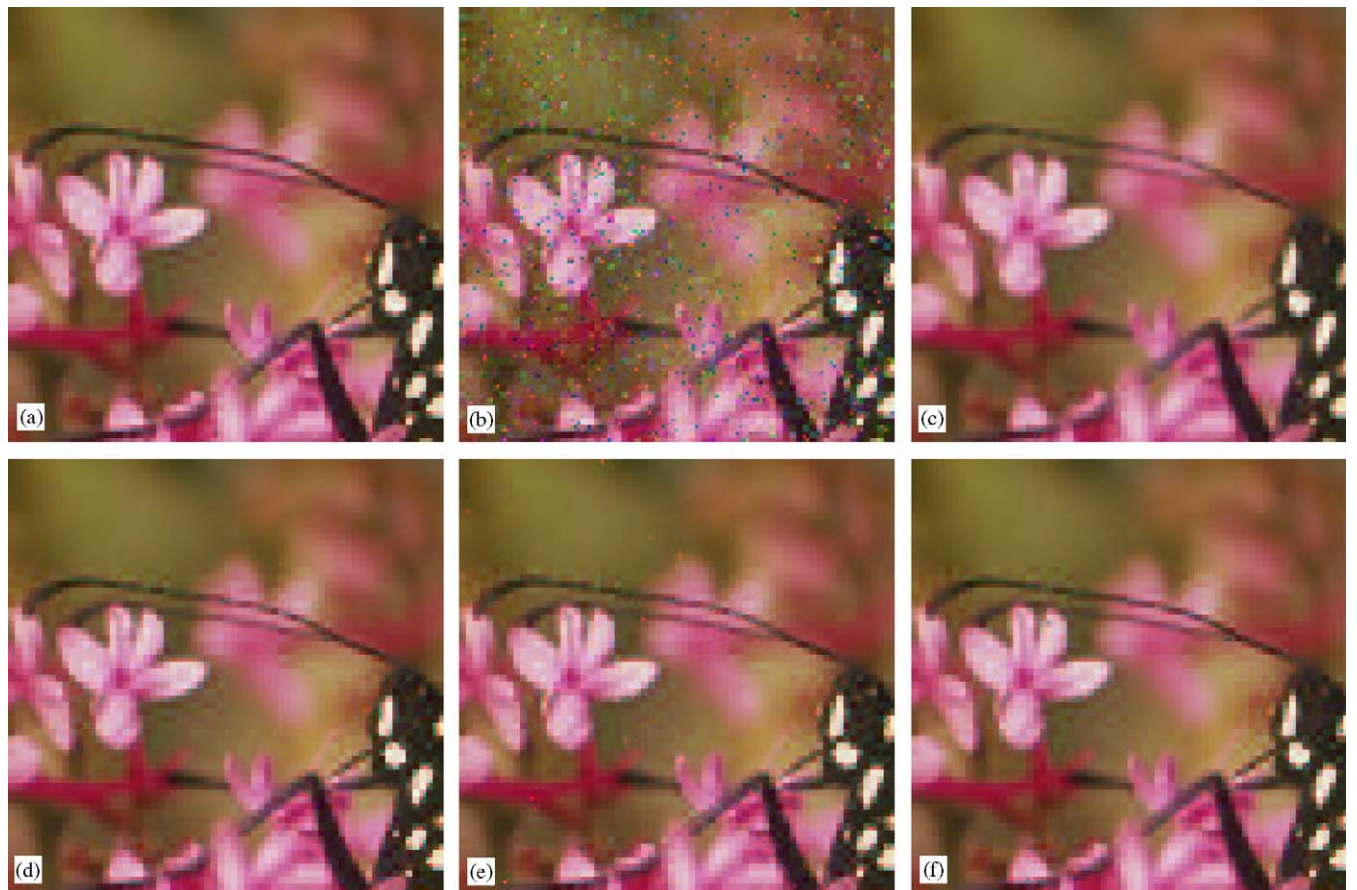


Fig. 12. The zoomed reconstruction of the NEAVF filter compared with other techniques, where the image *Monarch* is corrupted by 10% impulse noise: (a) original, (b) corrupted, (c) VMF output, (d) SAA output, (e) SCWVDF output and (f) NEAVF output.

the performances of noise detection and detail preservation. The parameters of the filter are well adapted to the input image and noise characteristics, and the implementation of the filter can be designed to achieve a high computation efficiency. The new filter has been compared with other prior-art techniques and demonstrated a noticeable gain in terms of noise detection accuracy, objective distortion measures, and perceptual visual quality.

References

- [1] Plataniotis KN, Venetsanopoulos AN. Color image processing and applications. Berlin: Springer; 2000.
- [2] Lukac R, Smolka B, Martin K, Plataniotis KN, Venetsanopoulos AN. Vector filtering for color imaging. *IEEE Signal Processing Magazine* 2005;22(1):74–86.
- [3] Plataniotis KN, Venetsanopoulos AN. Vector processing. In: Sangwine SJ, Horne REN, editors. Colour image processing handbook. London: Chapman & Hall; 1997. p. 188–209.
- [4] Hardie RC, Arce GR. Ranking in R^p and its use in multivariate image estimation. *IEEE Transactions on Circuits Systems for Video Technology* 1991;1(2):197–209.
- [5] Pitas I, Tsakalides P. Multivariate ordering in color image filtering. *IEEE Transactions on Circuits Systems for Video Technology* 1991;1(3):247–59.
- [6] Tang K, Astola J, Neuvo Y. Nonlinear multivariate image filtering techniques. *IEEE Transactions on Image Processing* 1995;4(6):788–98.
- [7] Astola J, Haavisto P, Neuvo Y. Vector median filter. *Proceedings of the IEEE* 1990;78(4):678–89.
- [8] Trahanias PE, Venetsanopoulos AN. Vector directional filters: a new class of multichannel image processing filter. *IEEE Transactions on Image Processing* 1993;2(4):528–34.
- [9] Karakos DG, Trahanias PE. Combining vector median and vector directional filters: the directional-distance filter. In: Proceedings of the IEEE international conference on image processing (ICIP'95), vol. 1, Washington DC, 1995. p. 171–174.
- [10] Gabbouj M, Cheikh FA. Vector median-vector directional hybrid filter for color image restoration. In: Proceedings of the EUSIPCO, vol. 2, Trieste, Italy, 1996. p. 879–881.
- [11] Viero T, Oistamo K, Neuvo Y. Three-dimensional median-related filters for color image sequence filtering. *IEEE Transactions on Circuits and Systems* 1994;4(2):129–42.
- [12] Alparone L, Barni M, Bartolini F, Caldelli R. Regularization of optic flow estimates by means of weighted vector median filtering. *IEEE Transactions on Image Processing* 1999;8(10):1462–7.
- [13] Lukac R, Smolka B, Plataniotis KN, Venetsanopoulos AN. Selection weighted vector directional filter. *Computers and Visual Image Understanding* 2004;94(1–3):140–67.
- [14] Lukac R, Plataniotis KN, Smolka B, Venetsanopoulos AN. Generalized selection weighted vector filter. *EURASIP Journal on Applied Signal Processing* 2004;12(2004):1870–85.
- [15] Lucat L, Siohan P, Barbac D. Adaptive and global optimization methods for weighted vector median filters. *Signal Processing: Image Communication* 2002;17(7):509–24.
- [16] Lukac R, Plataniotis KN, Smolka B, Venetsanopoulos AN. Weighted Vector median optimization. In: Proceedings of the fourth EURASIP conference video/image processing and multimedia communications, vol. 1, 2003. p. 227–232.
- [17] Plataniotis KN, Vinayagamoorthy S, Androutsos D, Venetsanopoulos AN. An adaptive nearest neighbor multichannel filter. *IEEE Transactions on Circuits Systems for Video Technology* 1996;6(6):699–703.
- [18] Plataniotis KN, Androutsos D, Venetsanopoulos AN. Color image processing using adaptive vector directional filters. *IEEE Transactions on Circuits and Systems II* 1998;45(10):1414–9.
- [19] Lin RS, Hsueh YC. Multichannel filtering by gradient information. *Signal Processing* 2000;80(2):279–93.
- [20] Szczepanski M, Smolka B, Plataniotis KN, Venetsanopoulos AN. On the geodesic paths approach to color image filter. *Signal Processing* 2003;83(6):1309–42.
- [21] Ma Z, Wu HR, Qiu B. A window adaptive hybrid vector filter for color image restoration. In: Proceedings of the IEEE international conference on acoustics, speech, and signal processing (ICASSP'04), vol. 3, Montreal, Canada, 2004. p. 205–208.
- [22] Ma Z, Wu HR, Qiu B. An structure adaptive hybrid vector filter for the restoration of digital color images. *IEEE Transactions on Image Processing*, October 2004, accepted for publication.
- [23] Plataniotis KN, Androutsos D, Venetsanopoulos AN. Adaptive fuzzy systems for multichannel signal processing. *Proceedings of the IEEE* 1999;87(9):1601–22.
- [24] Chatzis V, Pitas I. Fuzzy scalar and vector median filters based on fuzzy distances. *IEEE Transactions on Image Processing* 1999;8(5):731–4.
- [25] Tsai HH, Yu PT. Genetic-based fuzzy hybrid multichannel filters for color image restoration. *Fuzzy Sets and Systems* 2000;114(2):203–24.
- [26] Khriji L, Gabbouj M. Adaptive fuzzy order statistics-rational hybrid filters for color image processing. *Fuzzy Sets and Systems* 2002;128(1):35–46.
- [27] Hore ES, Qiu B, Wu HR. Improved color image vector filtering using fuzzy noise detection. *Optical Engineering* 2003;42(6):1656–64.
- [28] Lukac R, Plataniotis KN, Smolka B, Venetsanopoulos AN. cDNA microarray image processing using fuzzy vector filtering framework. *Journal of Fuzzy Sets and Systems: Special Issue on Fuzzy Sets and Systems in Bioinformatics* 2005;152(1):17–35.
- [29] Hore ES, Qiu B, Wu HR. Prediction based image restoration using a multiple window configuration. *Optical Engineering* 2002;41(8):1–11.
- [30] Lukac R, Marchevsky S. Adaptive vector LUM smoother. In: Proceedings of the IEEE international conference on image processing (ICIP'01), vol. 1, 2001, pp. 878–881.
- [31] Lukac R. Adaptive vector median filtering. *Pattern Recognition Letters* 2003;24(12):1889–99.
- [32] Lukac R. Adaptive color image filtering based on center-weighted vector directional filters. *Multidimensional Systems and Signal Processing* 2004;15(2):169–96.
- [33] Ma Z, Wu HR. Classification based adaptive vector filter for color image restoration. In: Proceedings of the IEEE international conference on acoustics, speech, and signal processing (ICASSP'05), vol. 2, Philadelphia, USA, 2005. p. 617–620.
- [34] Ma Z, Wu HR. Partition based vector filtering technique for noise suppression in digital color images. *IEEE Transactions on Image Processing*, submitted for publication.
- [35] Smolka B, Chydzinski A, Wojciechowski K, Plataniotis KN, Venetsanopoulos AN. Self-adaptive algorithm for impulsive noise reduction in color images. *Pattern Recognition* 2002;35(8):1771–84.
- [36] Smolka B, Lukac R, Chydzinski A, Plataniotis KN, Wojciechowski K. Fast adaptive similarity based impulse noise reduction filter. *Real-Time Imaging Special Issue on Spectral Imaging* 2003;9(4):261–76.
- [37] Davies ER. Accuracy of multichannel median filter. *IEE Electronics Letters* 2000;36(25):2068–9.
- [38] Astola J, Kuosmanen P., editors. Fundamentals of nonlinear digital filtering. Boca Raton, FL: CRC; 1997.
- [39] Ma Z, Wu HR. A histogram based adaptive vector filter for color image restoration. In: Proceedings of the IEEE fourth international conference on information and communication

- signal processing & fourth pacific-rim conference on multimedia (ICICS-PCM'03), Singapore, 2003. p. 1A3.4.1–5.
- [40] Huber PJ, editor. Robust statistics, New York: Wiley; 1981.
- [41] David HA, editor. Order statistics, New York: Wiley; 1981.
- [42] Kuwahara M, Hachimura K, Eiho S, Kinoshita M. Processing of RI-angiographic images. Digital processing of biomedical images. New York: Plenum; 1976. p. 187–203.
- [43] Nagao M, Matsuyama T. Edge preserving smoothing. Computer Graphics and Image Processing 1979;9(4):394–407.
- [44] Bakker P, van Vliet L, Verbeek PW. Edge preserving orientation adaptive filtering. In: Proceedings of the IEEE-CS conference on computer vision and pattern recognition, Los Alamitos, CA, 1999. p. 535–540.
- [45] Press WH, Teukolsky SA, Vetterling WT, Flannery BP, editors. Numerical recipes in C. Cambridge: Cambridge University Press; 1999.
- [46] Barni M, Cappellini V. On the computational complexity of multivariate median filters. Signal Processing 1998;71(1):45–54.